RSC Advances

PAPER

View Article Online
View Journal | View Issue

Cite this: *RSC Adv.*, 2014, **4**, 32276

Silver-coordination polymer network combining antibacterial action and shape memory capabilities†

Lin Wang, Wenxi Wang, Shubin Di, Xifeng Yang, Hongmei Chen, Tao Gong and Shaobing Zhou*

Received 26th April 2014
Accepted 24th June 2014

DOI: 10.1039/c4ra03829k

www.rsc.org/advances

In this study, a multifunctional polymer network is achieved by first synthesizing an isonicotinate-functionalized polyester (PIE) *via* classical melt-condensation polymerization, and secondly, the pendant of the pyrazinamide groups on the polyester side chains is coordinated with Ag ions to form a physically cross-linked network. Thermo property analysis and dynamic mechanical analysis reveal that the Ag-coordination polymer network possesses an excellent thermo-induced shape memory function, both under air and physiological conditions, due to a wide glass transition temperature region. The Ag ion concentration coordinated with the polymer was optimized to achieve the best shape memory effect using atomic absorption spectrometry. Moreover, the coordinated polyester can act as a reservoir of bactericidal Ag ions, in which the Ag ions are released and measured with inductively coupled plasma mass spectrometry, and in turn the antibacterial function is realized. Finally, the result of an Alamar blue assay reveals that the Ag-coordinated polyester has good cytocompatibility despite the introduction of a certain amount of Ag ions. Therefore, the multifunctional polymer has great potential applications in the biomedical field, *e.g.*, burn wound dressings.

Introduction

Shape memory polymers (SMPs) are a class of stimuli-sensitive materials that can memorize a temporary shape and recover their initial shape in response to an environmental stimulus.[1–3] To date, SMPs have been widely investigated for their great potential applications in biomedical devices, especially the thermo-induced SMPs.[4,5] These polymers can be deformed into a compact form, or other forms, according to the need of surgery and in turn, the shape memory function probably allows them to be delivered both conveniently and safely, and subsequently recover to complex final shapes *in vivo* upon exposure to body temperature.[6] Generally, SMPs consist of a fixity phase for the recovery of their initial shape and a reversible phase for the formation and fixation of the temporary shape.[7] The fixity phase is either a chemical cross-linking or physical cross-linking structure. Generally, the chemical cross-linking structure contains active chemical groups such as diisocyanate and cinnamon groups,[8,9] and the physical cross-linking structure contains an entanglement of molecular chains or hydrogen bonding.[10–13]

Most recently, metal–ligand coordinations have been utilized to form new physical cross-linking structures and obtain shape memory hydrogels. For example, Liu *et al.* reported a shape memory hydrogel with an imidazole–zinc ion coordination[14] and triple-shape memory poly (acrylonitrile 2-methacryloyloxyethyl phosphorylcholine) based on the dipole–dipole-zinc ion coordination.[15] In contrast to the chemical cross-linking or physical cross-linking structures previously reported, the formation of the metal–ligand coordination is simple and the conditions are mild. Metal–ligand coordination polymers are compounds containing the coordinative interaction of metal ions and charged or neutral organic ligands.[16,17] The ligands mainly include N-donor ligands. Among these ligands, reactive pendant isonicotinic acid groups are widely used as a kind of pyridinium-type ligand.[18] Silver ions are considered as ideal candidates to form coordination polymers. In addition, they have one of the highest levels of toxicity for microorganisms, but the least toxicity for eukaryotic cells.[19] Ag is used in many cases for disinfection, and polymer complexes with Ag ions have great potential for applications in medical instruments.[20–24] Moreover, the mechanism of antibacterial action and clinical toxicology have been reviewed systematically.[25–27]

In this study, our concept for implementing a combination of the antibacterial action and the shape memory capabilities is a silver-coordination polymer network. This network is fabricated on the basis of Ag-coordinated isonicotinate-

Key Laboratory of Advanced Technologies of Materials, Ministry of Education, School of Materials Science and Engineering, Southwest Jiaotong University, Chengdu, Sichuan 610031, PR China. E-mail: shaobingzhou@swjtu.edu.cn

† Electronic supplementary information (ESI) available. See DOI: 10.1039/c4ra03829k

functionalized polyester (PIE) (Ag–PIE), in which pyrazinamide groups located in the polymer side chains provide a ligand effect. The low toxicity of isonicotinic acid has been verified by previous research.[28] Since the Ag-coordinated polyester has a physical cross-linking structure, it displays good shape memory function. Simultaneously, the polymer network is endowed with antibacterial properties due to the introduction of Ag ions. The coordinated polyester can act as a reservoir of bactericidal Ag ions, in which they are released, and in turn the antibacterial functions will be realized.

Experimental section

Materials

Isonicotinic acid, sebacic acid and diethanolamine (DEA) were purchased from the Kelong chemical reagent factory in Chengdu (China). The sebacic acid was recrystallized before use. The other chemical reagents were of reagent grade and used without further purification. The cells belonged to normal neonatal rat mandibular cell lines, which were passaged to the third generation just before our experiments. *Escherichia coli* (*E. coli*, ATCC 25922) was selected for the antibacterial experiment.

Preparation of *N*,*N*-bis (2-hydroxyethyl) pyrazinamide (BIN)

BIN was synthesized through an aminolysis reaction from methyl isonicotinate and DEA, as shown in Scheme 1A. Firstly, methyl isonicotinate was synthesized from isonicotinic acid and methanol under a H_2SO_4 catalyst in 60 °C for 4 h. After the reaction was completed and cooled to room temperature, $NaHCO_3$ solution was added into the reaction liquid until it was neutral, and then methyl isonicotinate was extracted from the solution by methylene chloride. After that, BIN was synthesized from methyl isonicotinate and DEA under Ar at 90 °C for 24 h. Finally, BIN in form of a white solid was obtained from crude product by washing with deionized water.

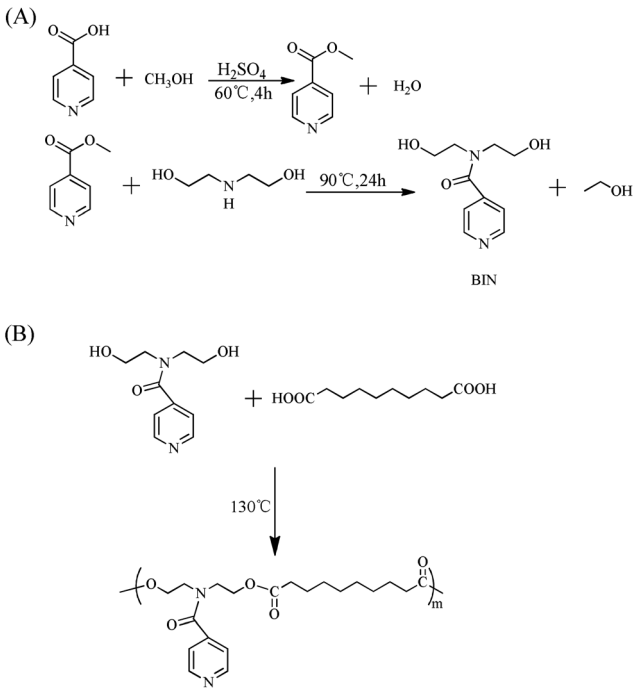

Scheme 1 Synthetic routes of BIN (A) and PIE (B).

Preparation of polyester (PIE)

The PIE was synthesized through melt phase polycondensation, as shown in Scheme 1B. Briefly, 10 mmol BIN and 10 mmol sebacic acid were combined by melting at 130 °C under a blanket of Ar. Then a polycondensation reaction was carried out under reduced pressure for 24 h. A transparent light yellow viscous product was obtained. After the reaction, the viscous product was poured into a PTFE mold and a PIE film was obtained when it cooled. The molecular weight of PIE, measured by GPC, was 45 200, and the polydispersity was 1.467.

Preparation of Ag–PIE

Firstly, the polymer was soaked in 4 g L^{-1} $AgNO_3$ solution for 1 h, then the water was wiped off the surface and dried further under vacuum, at room temperature for 24 h. Finally, the Ag–PIE films were prepared for DMA, a shape memory test, and an antibacterial performance test.

The absorption of Ag ions

The Ag–PIE samples were immersed in 20 mL 4 g L^{-1} $AgNO_3$ solution for 1 h, and the $AgNO_3$ solution were analyzed with Atomic Absorption Spectrometry (AAS, Thermo Elemental S4) at the designated time.

Ag ion release

The Ag ion release from the Ag–PIE was measured with Inductively Coupled Plasma Mass Spectrometry (ICP, NexION 300X). The Ag–PIE samples were immersed in 10 mL of phosphate buffer solution (PBS) at 25 °C and 37 °C for 24 h. When the Ag–PIE samples were immersed in PBS for 2 h, 4 h, 8 h, 16 h, 24 h, and 30 h, 2 mL PBS was pipetted at each time point. Then the PBS solutions containing the released Ag ions were measured by ICP at the designed time.

Characterisation

FT-IR was measured by a Nicolet 5700 IR spectrometer. All the samples were obtained by using KBr plates, in which dry powder was mixed with KBr at a weight ratio of 0.5–1%. ^{1}H-NMR spectra were obtained on a Bruker AM-300 spectrometer. Tetramethylsilane (TMS) was used as the internal standard and $CDCl_3$ was used as the solvent. The thermal properties of the polymers were determined by DSC (TA DSC-Q100). In order to eliminate any unknown thermal histories of the samples, heating and cooling were repeated from −20 °C to 120 °C, and the DSC curves of the second heating and cooling process were obtained. Both the heating and cooling ratios were 10 °C min^{-1}. All the data were used from the second heating process. DMA was carried out using a specimen with a size of 10 × 3 × 1 mm (length × width × thickness) and a DMA instrument (TA DMA-Q 800), at a heating ratio of 3 °C min^{-1} from 0 to 80 °C and a frequency of 1

Hz. The storage modulus E' and tan delta were tested. Gel permeation chromatography (GPC) was performed with a Water 2695 separation module equipped with a StyragelHT4DMF column, calibrated with polystyrene narrow standards operated at 40% and a series 2414 refractive index detector.

Investigation of the thermo-induced shape memory effect

The thermo-induced shape memory properties were measured using strip specimens of the Ag–PIE. The strips was heated to 50 °C for 1 min so that they could be softened, and were bent into a spiral shape, named the temporary shape. Then, the deformed specimen was moved to 0 °C ice water for 1 min for freezing stress and fixation of the deformed shape. When the spiral shape specimen was induced with 40 °C hot air, recovery to its initial shape could be observed.

The shape memory fixity ratio and recovery ratio were measured using strip shaped specimens measured by DMA with a controlled force mode, according to our designed experiment. A typical testing procedure was performed as previously reported.[29] Firstly, straining the specimen at a constant stress rate at 45 °C obtained a temporary shape, marked as ε_1. The specimen was then cooled to 0 °C and the stress was released, marked as ε_2. Secondly, the temporary shape was heated from 0 °C to 45 °C, and the was strain marked as ε_0. The shape memory fixity ratio and recovery ratio were calculated according to the following equations:

$$R_f = \frac{\varepsilon_2}{\varepsilon_1} \times 100\% \quad (1)$$

$$R_r = \left(1 - \frac{\varepsilon_0}{\varepsilon_1}\right) \times 100\% \quad (2)$$

Antibacterial performance assay

Escherichia coli (ATCC 25922) was selected for the antibacterial experiment. Each specimen was sterilized with UV light for 24 h before the experiment. The antibacterial performance assays were evaluated based on two methods: a coating method and an Alamar blue assay, as previously reported.[30] The bacteria were cultivated in a beef extract-peptone (BEP) medium (GB/T 4789.28) at 37 °C for 12 h, and then 1 mL of the bacterial suspension was taken out and dispersed into 9 mL of PBS until the concentration of the bacterial suspension was adjusted to approximately 10^5 colony forming units (CFU mL^{-1}). Each sample was put in 5 mL of the bacterial suspension in the dark at 37 °C for 5 h. 100 μL of each bacterial suspension was then taken out and spread onto a nutrient agar plate with 10 mL medium/PBS. After that, the samples were incubated at 37 °C for 24 h. Finally, through the appearance of a bacteriostatic ring, the Alamar blue assay was carried out to investigate the antibacterial performance. A sample of 200 μL of reduced Alamar blue solution was pipetted into a costar opaque black bottom 96-well plate (Sigma) and read at 600 nm (emission) in an ELISA microplate reader (Molecular Devices, Sunnyvale, CA).

In vitro cytotoxicity assays

The cytotoxicity assays were evaluated based on the Alamar blue assay, as in our previous report.[31] In brief, all the samples were cut into small round flakes at an average diameter of nearly 12 mm to be used for osteoblast culture *in vitro*. Next, the osteoblasts were grown in RPMI medium 1640 (Gibcos) with 10% fetal bovine serum (FBS). These cells, with a density of 1×10^4 cells per well, were cultured in 24-well plates (Sigma) in the above medium and maintained at 37 °C in a humidified incubator with 5% CO_2. At the predesigned time points of 1, 3, and 5 days, the medium was removed and 300 μL Alamar blue solution (10% Alamar blue, 80% media 199 (Gibcos) and 10% FBS; v/v) was added into each well and incubated for a further 3 h. Wells without materials were blank controls. A sample of 200 μL of reduced Alamar blue solution was pipetted into a costar opaque black bottom 96-well plate (Sigma) and read at 570 nm (excitation)/600 nm (emission) in an ELISA microplate reader (Molecular Devices, Sunnyvale, CA). Cell morphology and growth on the PIE films were evaluated by fluorescence microscopy (DMIL, Leica, Germany) and all the cells were stained by calcein.

Results and discussion

The isonicotinate-functionalized polyester (PIE) was synthesized *via* classical melt-condensation polymerization under high vacuum at 130 °C. The composition of the polyester and Ag-coordinated polyester were investigated using Fourier transform infrared spectroscopy (FT-IR) and proton nuclear magnetic resonance (^{1}H-NMR). Fig. S1 in the ESI† shows the FT-IR and ^{1}H-NMR spectra of *N*,*N*-bis (2-hydroxyethyl) pyrazinamide (BIN). The FTIR spectrum of BIN, as shown in Fig. S1A,† exhibits characteristic absorption peaks of C–N stretching vibration at 1470 cm^{-1} and the N–C=O stretching vibration at 1620 cm^{-1}. In the ^{1}H-NMR of BIN (Fig. S1B†), the chemical shifts at 3.15 ppm, 3.61 ppm, 7.81 ppm and 8.89 ppm are attributed to –N–CH_2–, –CH_2–OH and pyridine H atoms, respectively. From the FT-IR spectra of PIE and Ag–PIE in Fig. S2,† we can clearly see that PIE exhibits characteristic absorption peaks of C–N stretching vibration at 1450 and 1490 cm^{-1}, while the red shift occurs in the FTIR spectrum of Ag–PIE due to the ligand coordinating with the Ag ion, indicating that the coordination polymer has been synthesized successfully. From the results of Fig. S3 in the ESI,† we can observe that there is an obvious difference in transmittance. In the UV-vis curve of Ag–PIE, there is a maximum transmissive peak at 410 nm, owing to the Ag ions. The changes in PIE and Ag–PIE, from the FTIR and UV-vis results, indicate that the coordination polymer was prepared successfully.

The thermal transition temperatures of PIE and Ag–PIE were investigated by differential scanning calorimetry (DSC) analysis using the second heating thermogram. It can be observed from Fig. 1A that all the specimens show a wide glass transition temperature region from 20 °C to ~80 °C. To verify the amount of adsorbed Ag ions, thermogravimetric (TG) analysis was carried out, and the results are presented in Fig. 1B. The TG curve of PIE shows a weight loss of 98% from 0 °C to 500 °C for the decomposition of PIE, however, for Ag–PIE, the temperature of decomposition increases, suggesting

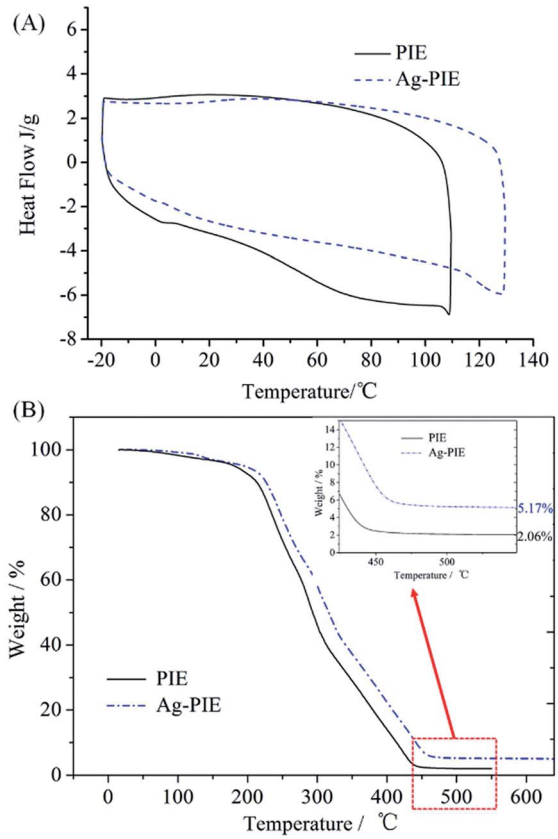

Fig. 1 DSC (A) and TG (B) curve of PIE and Ag–PIE. Inset highlights weight loss that occurred at 500 °C.

that the polyester coordinated with Ag ions has a better stability. From the weight loss, the concentration of adsorbed Ag ions in this polymer network could be calculated and was found to be about 3.11%.

The dynamic mechanical behavior depending on temperature is an important factor for the investigation of SMPs, because it could predict shape memory properties and provide information for shape fixity and recovery.[32] Fig. 2 shows the storage modulus and tan delta curves of PIE and Ag–PIE. At lower temperatures, the Ag–PIE has a higher storage modulus (1130 MPa) than that of the initial polymer (950 MPa). A high glassy-state modulus would provide the material with a good shape fixity when cooled, but a high rubbery modulus could lead to a large elastic recovery at high temperatures.[33] This theory is a basic condition of shape memory polymers.[34] Based on these guidelines, we can infer that Ag–PIE possesses an excellent shape memory effect. Furthermore, from the tan delta results, we can observe that Ag–PIE has a higher transition temperature from 20 °C to 55 °C than the transition temperature of PIE, which is consistent with the DSC analysis results. The wide glass transition temperature region could provide the deformed and recovery temperatures for the shape memory process.

The thermo-induced shape memory effect of Ag–PIE was further investigated by dynamic mechanical analysis (DMA) with a controlled force mode. The quantitative demonstration

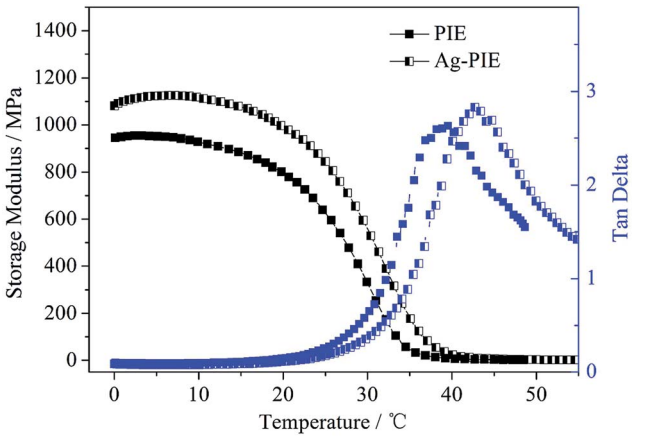

Fig. 2 DMA curves of the PIE and the Ag–PIE.

of the thermo-induced shape memory properties of Ag–PIE is shown in Fig. 3A. In the stress–strain–temperature curves, Ag–PIE exhibits an excellent shape memory effect, and the shape fixity ratio and recovery ratio remain above 95%, as calculated from the eqn (1) and (2). Moreover, from the shape memory fixity and recovery process of Ag–PIE (Fig. 3B), we can also see that Ag–PIE exhibits good shape fixity and shape recovery ratios. Analysis of all the samples was repeated three times, and both the shape fixity and recovery ratios remain more than 95%.

The proposed thermo-induced shape memory mechanism for Ag–PIE is shown in Scheme 2. In this shape memory system, the pyrazinamide groups introduced into the polymer side chains provide the ligands. Later, after PIE is immersed in $AgNO_3$ solution, with the solution penetrating into the polymer matrix, the ligands of PIE can easily coordinate with

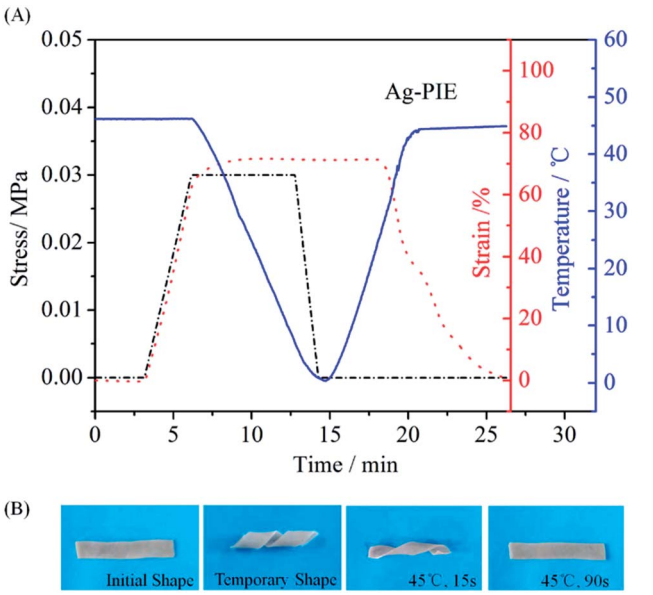

Fig. 3 Shape memory properties of Ag–PIE measured by DMA (A); shape memory fixing and recover process (B).

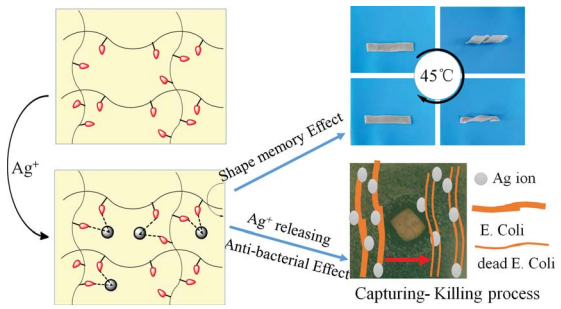

Scheme 2 The mechanisms of shape memory and the antibacterial effect of Ag–PIE.

Ag ions to form a physical cross-linking structure. In the process of shape memory, the physical cross-linking structure can act as the fixity phase to provide the elasticity for recovering their initial shape. The polyester molecular chains act as the reversible phase for the formation and fixation of the temporary shape.

The Ag ion concentration coordinated with the polymer was further optimized to achieve the best shape memory effect. The absorption of Ag ions was measured by Atomic Absorption Spectrometry (AAS, Thermo Elemental S4). The Ag–PIE film samples were first immersed in 20 mL 4 g L^{-1} $AgNO_3$ solution at 22 °C for 15 min, 30 min, 45 min, 60 min, and 75 min. Then, the accumulated amount of absorbed Ag ions after the designated time was analyzed by AAS. In Fig. 4, it can be observed that with the increase in immersion time, the amount of absorbed Ag ions increases to about 5 mg g^{-1} (Ag ion/PIE) at 60 min. After that, the amount of Ag ions remains almost unchanged. Therefore, Ag–PIE immersion for 60 min was selected for all investigations.

The effect of the amount of absorbed Ag ions on shape memory was investigated. In Fig. 4, the shape fixity rate and the shape recovery rate increase with increasing absorbed Ag ions, which is also due to the increasing cross-linking effect from the coordination with Ag ions. When the amount of absorbed Ag ions reached about 5 mg g^{-1}, as obtained from AAS analysis, the maximum shape fixity and recovery rate could be achieved.

Additionally, as a potential biomedical material, the investigation of shape memory effect on to physiological conditions is necessary. The shape memory process for Ag–PIE in phosphate buffer solution (PBS) at 37 °C is shown in Fig. 5A. It can be found that Ag–PIE also possess good shape memory properties, and it can recover its initial shape within 60 s. Fig. 5B shows the DSC curves of Ag–PIE and the sample immersed in PBS for 1 min. The results indicate that there is a pronounced decrease in the transition temperature after immersion in PBS for 1 min due to the absorption of water. The faster recovery of the immersed sample can be ascribed to the decrease of the transition temperature.

For medical devices, the antibacterial function is vital for resisting bacterial infection when implanting *in vivo*. The antibacterial properties of Ag–PIE were investigated. Firstly, the release of Ag ions from Ag–PIE at 25 °C for storage and 37 °C for *in vivo* applications were studied using Inductively Coupled Plasma Mass Spectrometry (ICP, NexION 300X). As shown in Fig. 6A, the concentration of the released Ag ions at 25 °C could reach 0.61 mg L^{-1} after 24 h, while the concentration of the released Ag ions at 37 °C were 0.18 mg L^{-1} after 2 h and up to 0.91 mg L^{-1} after 24 h. Ag ions can damage bacterial cell membranes and thus alter their function, but the cytotoxicity to normal cells cannot be ignored. The maximum Ag ion concentration has been reported to be less than 10 mg L^{-1}.[35] In our study, the accumulated release amount of Ag ions both at 25 and 37 °C is much less than 10 mg L^{-1}, so we think that Ag–PIE can be potentially applied as a biomaterial.

Fig. 6B shows the antibacterial effect of Ag–PIE against *Escherichia coli*. Without the Ag coordination, PIE did not have any effect on the bacterial growth, while Ag–PIE had obvious

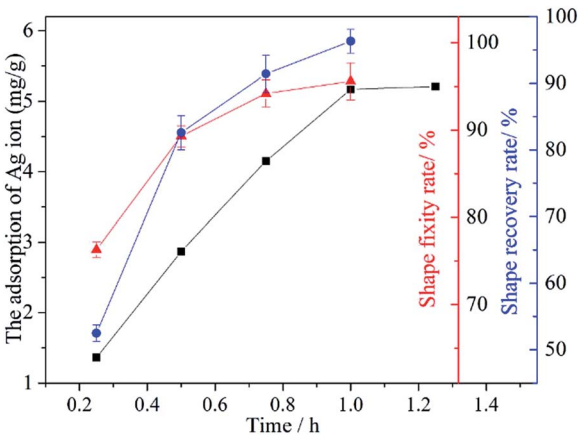

Fig. 4 Shape fixity and shape recovery ratio under different amounts of absorbed Ag ions.

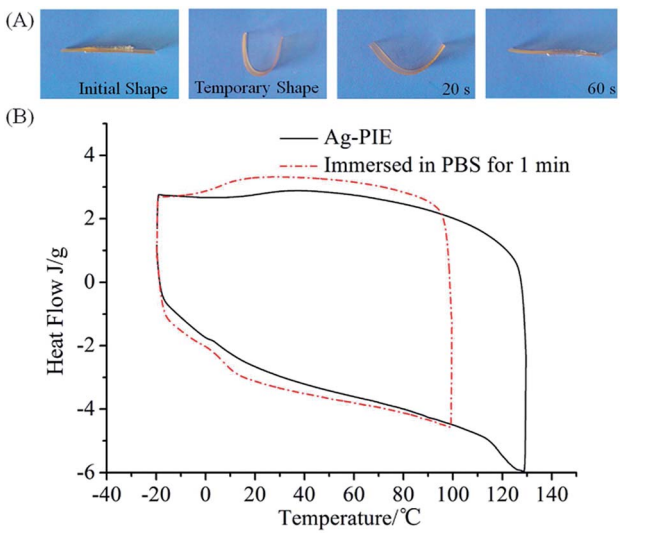

Fig. 5 Shape memory effect of Ag–PIE in PBS at 37 °C (A); DSC curves of Ag–PIE before and after immersion in PBS for 1 min (B).

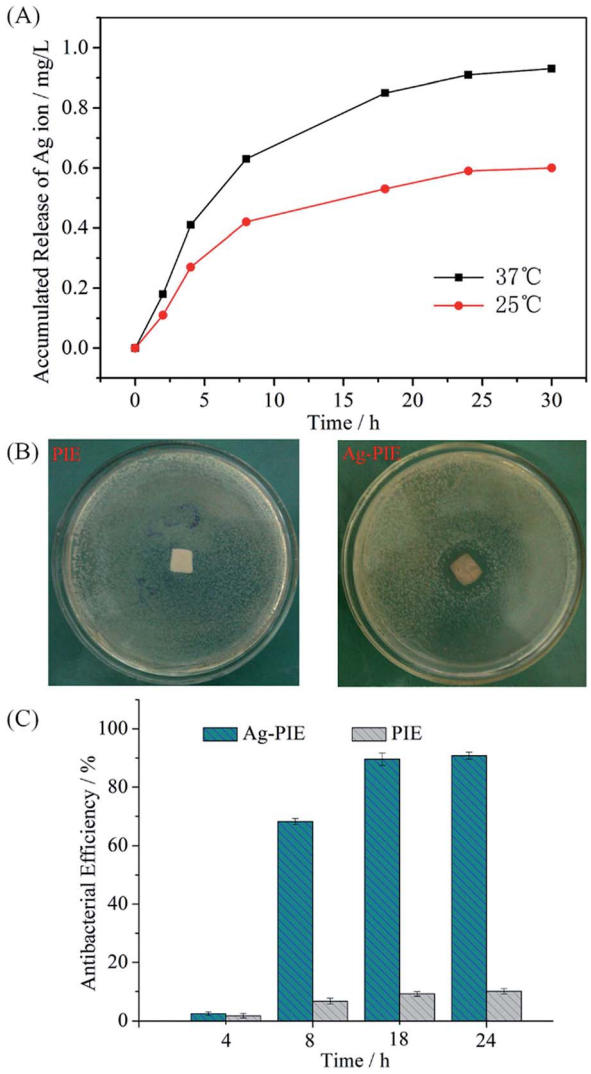

Fig. 6 Ag ion release profiles in PBS at 37 °C and 25 °C (A), bacterial colonies of PIE and Ag–PIE (B) and the antibacterial efficiency of Ag–PIE compared with PIE against *E. coli* (C).

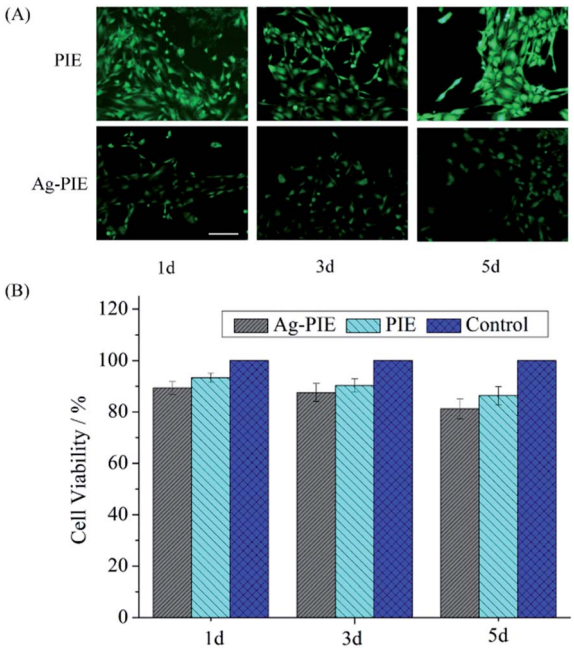

Fig. 7 (A) Fluorescence images showing the osteoblasts cultured on the PIE and Ag–PIE substrates at day 1, day 3, and day 5; cells were strained by calcein and all the scale bars represent 25 μm. (B) Cell viability.

antibacterial activity. Fig. 6C shows the antibacterial activity of the samples against *Escherichia coli* in the fluid culture medium at 37 °C. We can see that Ag–PIE has an antibacterial efficiency of 92% after 24 h. The proposed antibacterial shape memory mechanism for Ag–PIE is shown in Scheme 2. Ag ions could be released from the coordinated polyester to provide the antibacterial effect.

The excellent non-cytotoxicity is an important characteristic of biomaterials. Therefore, *in vitro* cytotoxicity of PIE and Ag–PIE was further assessed by measuring the viability of osteoblast cells with an Alamar blue assay. From Fig. 7B, it can be observed that the cell viability remained greater than 85% for all specimens, and moreover, the viability in the Ag–PIE group was not significantly different from that of the cells cultured on PIE. This result indicates that PIE coordinated with a certain amount of Ag ions can still have good cytocompatibility. The morphology of osteoblasts was observed by fluorescence microscopy after being stained by calcein, as shown in Fig. 7A. It can be clearly seen that the osteoblasts grew healthily and attached well on the all films. It also demonstrated that the concentration of the released Ag ions is almost nontoxic to cells. Therefore, the Ag-coordination polymer network, combining antibacterial action and shape memory capabilities, is potentially suitable for applications in medicine.

Conclusion

In summary, we originally developed one type of silver-coordination polymer network combining excellent shape memory function and highly antibacterial action *via* a simple strategy. In this polymer network, the pyrazinamide groups located in the polymer side chains provide a ligand effect with the absorbed Ag ions to endow the shape memory function, and the coordinated polyester acts as a reservoir of Ag ions to allow them be gradually released. By quantitatively optimizing the Ag ion amount in the polymer network, a good balance was achieved between the antibacterial action, shape memory function and cytocompatibility. The multifunctional polymer has great potential for applications in smart medical devices.

Acknowledgements

This work was partially supported by the National Basic Research Program of China (973 Program, 2012CB933600), the National Natural Science Foundation of China (no. 30970723 and no. 51173150), the Research fund for the Doctoral Program of Higher Education of China (20120184110029) and the Construction Program for Innovative Research Team of University in Sichuan Province (14TD0050).

Notes and references

1 A. Lendlein and S. Kelch, *Angew. Chem., Int. Ed.*, 2002, **41**, 2034.
2 M. Behl and A. Lendlein, *Mater. Today*, 2007, **10**, 20.
3 H. Xu, C. Yu, S. Wang, V. Malyarchuk, T. Xie and J. A. Rogers, *Adv. Funct. Mater.*, 2013, **23**, 3299.
4 A. Beilvert, F. Chaubet, L. Chaunier, S. Guilois, G. Pavon-Djavid, D. Letourneur, A. Meddahi-Pellé and D. Lourdin, *Carbohydr. Polym.*, 2014, **99**, 242.
5 K. Kratz, U. Voigt and A. Lendlein, *Adv. Funct. Mater.*, 2012, **22**, 3057.
6 X. Liu, K. Zhao, T. Gong, J. Song, C. Bao, E. Luo, J. Weng and S. Zhou, *Biomacromolecules*, 2014, **15**, 1019.
7 J. Leng, X. Lan, Y. Liu and S. Du, *Prog. Mater. Sci.*, 2011, **56**, 1077.
8 Y. Shao, C. Lavigueur and X. X. Zhu, *Macromolecules*, 2012, **45**, 1924.
9 L. Wang, X. Yang, H. Chen, T. Gong, W. Li, G. Yang and S. Zhou, *ACS Appl. Mater. Interfaces*, 2013, **5**, 10520.
10 W. Voit, T. Ware, R. R. Dasari, P. Smith, L. Danz, D. Simon, S. Barlow, S. R. Marder and K. Gall, *Adv. Funct. Mater.*, 2010, **20**, 162.
11 X. Zheng, S. Zhou, X. Li and J. Weng, *Biomaterials*, 2006, **27**, 4288.
12 D. J. Davies, A. R. Vaccaro, S. M. Morris, N. Herzer, A. P. Schenning and C. W. Bastiaansen, *Adv. Funct. Mater.*, 2013, **23**, 2723.
13 S. Zhou, X. Zheng, X. Yu, J. Wang, J. Weng, X. Li, B. Feng and M. Yin, *Chem. Mater.*, 2007, **19**, 247.
14 W. Nan, W. Wang, H. Gao and W. Liu, *Soft Matter*, 2013, **9**, 132.
15 Y. Han, T. Bai, Y. Liu, X. Zhai and W. Liu, *Macromol. Rapid Commun.*, 2012, **33**, 225.
16 J. R. Kumpfer and S. J. Rowan, *J. Am. Chem. Soc.*, 2011, **133**, 12866.
17 I. Chevrier, J. L. Sagué, P. S. Brunetto, N. Khanna, Z. Rajacic and K. M. Fromm, *Dalton Trans.*, 2013, **42**, 217.
18 A. Muñoz-Bonilla and M. Fernández-García, *Prog. Polym. Sci.*, 2012, **37**, 281.
19 S. Chernousova and M. Epple, *Angew. Chem., Int. Ed.*, 2013, **52**, 1636.
20 K. M. Fromm, *Appl. Organomet. Chem.*, 2013, **27**, 683.
21 K. Wang, Y. Yin, C. Li, Z. Geng and Z. Wang, *CrystEngComm*, 2011, **13**, 6231.
22 V. W. L. Ng, J. P. K. Tan, J. Leong, Z. X. Voo, J. L. Hedrick and Y. Y. Yang, *Macromolecules*, 2014, **47**, 1285.
23 P. K. Fyfe, V. A. Rao, A. Zemla, S. Cameron and W. N. Hunter, *Angew. Chem.*, 2009, **121**, 9340.
24 A. Agarwal, K. M. Guthrie, C. J. Czuprynski, M. J. Schurr, J. F. McAnulty, C. J. Murphy and N. L. Abbott, *Adv. Funct. Mater.*, 2011, **21**, 1863.
25 J. S. Lee and W. L. Murphy, *Adv. Mater.*, 2013, **25**, 1173.
26 J. Maillard and P. Hartemann, *Crit. Rev. Microbiol.*, 2013, **39**, 373.
27 A. Alonso, X. Muñoz Berbel, N. Vigués, R. Rodríguez Rodríguez, J. Macanás, M. Muñoz, J. Mas and D. N. Muraviev, *Adv. Funct. Mater.*, 2013, **23**, 2450.
28 E. Torres, E. Moreno, S. Ancizu, C. Barea, S. Galiano, I. Aldana, A. Monge and S. Pérez-Silanes, *Bioorg. Med. Chem. Lett.*, 2011, **21**, 3699.
29 C. Liu, H. Qin and P. T. Mather, *J. Mater. Chem.*, 2007, **17**, 1543.
30 D. Ratna and J. Karger-Kocsis, *J. Mater. Sci.*, 2008, **43**, 254.
31 Y. Liu, K. Gall, M. L. Dunn and P. McCluskey, *Mech. Mater.*, 2004, **36**, 929.
32 A. Roguska, M. Pisarek, M. Andrzejczuk, M. Lewandowska, K. J. Kurzydlowski and M. Janik Czachor, *J. Biomed. Mater. Res., Part A*, 2012, **100**, 1954.
33 C. H. Kim, E. J. Choi and J. K. Park, *J. Appl. Polym. Sci.*, 2000, **77**, 2049.
34 C. Zhao, B. Feng, Y. Li, J. Tan, X. Lu and J. Weng, *Appl. Surf. Sci.*, 2013, **280**, 8.
35 S. Shao, S. Zhou, L. Li, J. Li, C. Luo, J. Wang, X. Li and J. Weng, *Biomaterials*, 2011, **32**, 2821.

